

# An Image Processing Algorithm for the In-vivo Quantification and Visualization of Septum Motion in Type III B - Aortic Dissections with Cine Magnetic Resonance Imaging

Christof Karmonik, Jean Bismuth, Mark G. Davies, Houssam K. Younes, Alan B. Lumsden

**Abstract**— Currently, there is no method to predict outcome of endovascular treatment (EVAR) of type III B aortic dissections (TB-AD). A new image processing algorithm is presented for quantifying IS displacement from cine 2D phase contrast magnetic resonance images (2D pcMRI) towards a new classification of TB-AD based on IS mobility,

Bulk motion of the true aortic lumen (tAB) center (ALC), maximum, minimum and average displacement of the boundary points composing the IS and tAB excluding the IS were quantified at two locations in one patient. Correlations of the ALC motion and the averaged temporal displacement AD(t) of IS and tAB excluding IS with the aortic flow waveform were calculated.

Range of ALC motion was similar in both locations ( average 0.56 mm, max 1.37 mm) and correlated with the aortic flow waveform in the abdominal aorta but not the thoracic aorta. Range of displacement of the IS was from 1.27 mm to -1.64 mm (average  $0.09 \pm 0.07$  mm) in the thoracic aorta, and from 0.38 mm to -3.38 mm (average  $0.42 \pm 0.23$  mm) in the abdominal aorta. tAB motion excluding the IS was 1.21 mm to 0.84 mm (thoracic, average  $0.13 \pm 0.07$  mm) and 0.52mm to -1.88 mm (abdominal, average  $0.37 \pm 0.11$  mm). AD(t) for IS and tAB excluding the IS both correlated with aortic flow in the abdominal aorta only.

## I. INTRODUCTION

**A**ORTIC dissections are blood-filled, axial separations between elastic laminae within the media. Rupture occurs in about 90 %. In 10 % of all cases, reentrant tears into the aortic lumen exist. The so created false lumen often re-endothelializes, however, often also thrombus formation is observed [1]. Type III Stanford B aortic dissections (TB-AD), which only involve the descending aorta are less lethal than other types [2,3].

Under the current classification system, TB-ADS are characterized by their clinical presentation. Those presenting less than 2 weeks from symptom onset are defined as acute, those that are symptomatic for 2 weeks or longer are considered chronic [4, 5]. At onset, the intra-arterial septum (IS) or intimal flap is believed to be thin expressing high mobility. At a later stage, the flap will have thickened and consequently, mobility will have decreased.

Manuscript received June 20, 2009.

All Authors are with the Methodist DeBakey Heart & Vascular Center, The Methodist Hospital, Houston, TX 77030. C.K. is also with The Methodist Hospital Neurological Institute (phone: 713-441-1583; fax: 713-790-2460; e-mail: ckarmonik@tmhs.org).

A new classification system of TB-AD based on the mobility of the IS is therefore warranted to predict outcome for EVAR treatment.

Magnetic resonance imaging (MRI), in contrast to computed tomography (CT) [6], contrast enhanced MRI [7] or digital subtraction angiography (DSA) [8-10], is capable of additionally visualizing motion in-vivo through 2-D phase contrast magnetic resonance imaging (2D pcMRI).

Towards a new classification system for EVAR treatment of TB-AD focusing on the IS mobility, we developed a semi-automated algorithm to parameterize true aortic lumen boundary (tAB) and IS motion based on 2D pcMRI cross sectional images of the aorta. The maximum distension, maximum contraction and average displacement of the tAB and the IS relative to the center of mass of the true aortic boundary points (ALC) are provided. Correlations of the average motion of the ALC, the tAB and the IS with the aortic blood flow waveform are calculated. The application of this algorithm is illustrated on two clinical 2D pcMRI cross sectional image sets acquired in the thoracic and in the abdominal aorta of a patient presenting with a TB-AD.

## II. METHODS

### A. 2D pcMRI Image Acquisition

Approval of the institutional review board was obtained for this retrospective study. From a patient diagnosed with TB-AD, two sets of 2D pcMRI images at 17 time points in the cardiac cycle (TR 41 ms, in-plane resolution 1.17x1.17 mm, VENC 150 cm/sec, slice thickness 5 mm, one breath hold) were acquired on a Siemens Sonata Magnetom 1.5 T human MRI scanner (Siemens, Medical Solutions, Erlangen, Germany). At location 1 (descending thoracic aorta), the false lumen of the aorta was patent and was partly thrombosed at location 2 (abdominal aorta).

A 3D surface reconstruction of the aortic lumen created from contrast-enhanced MR angiographic images (sagittal, in-plane resolution 1.04 mm x 1.04 mm, slice thickness 1.75 mm) served as a localizer to ensure that the position of the 2D pcMRI slices was perpendicular to the long axis of the aorta

### B. Segmentation of True Aortic Lumen Boundary

After magnifying the magnitude 2D pcMRI images

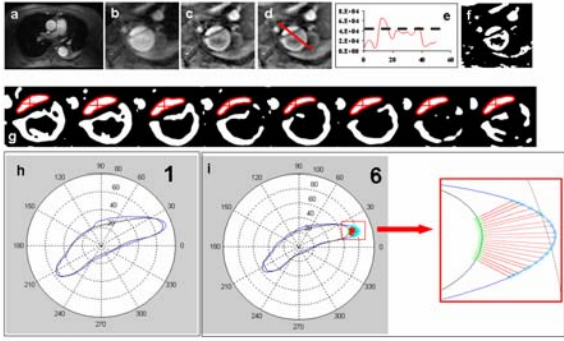


Fig. 1. *Top*: Illustration of the image post-processing algorithm: 2D magnitude pcMRI images (a) were enlarged by a factor 4 (b), bandpass filtered using a spatial Fourier transform (c), and median filtered to remove intensity inhomogeneities (d). Large contrast between the true aortic lumen and the aortic wall was achieved as visualized by the profile plot (e) of the image intensity across the red line in (d). (f) final mask after single value thresholding.

*Center*: Boundary of true aortic lumen (tAB) in red, with center of the tAB points (ALC) marked by red cross for selected images at different times during the cardiac cycle (g).

*Bottom*: Radial plot of tAB at minimum inflow (base boundary, black) and at time points 1 (h) and 6 (i) during the cardiac cycle (blue). Region in red box in (i) is enlarged on right. Normal vectors from selected points of the base boundary (green) to corresponding points of the tAB (magenta) are shown. Length of connecting distance between points (red) was identified as tAB displacement for each boundary point of the base boundary.

(figure 1a) by a factor of 4 using linear interpolation (figure 1b), images were modified with a Fourier spatial bandpass filter (ImageJ, version, 1.40g, NIH (<http://rsb.info.nih.gov/ij/>), figure 1c) to eliminate image intensity variation. Images were then filtered with a Median filter [11] to further homogenize image intensity inside the true aortic lumen. After these manipulations, the tAB could be segmented with conventional single value thresholding and seed point region growing (ImageJ, Wand tool, figure 1). The tAB identified in this way was stored as a polygonal regions of interest (pROI). pROI points and image data were imported into Matlab (Mathworks Inc.) for the following analysis.

### C. Calculation of Volumetric Blood Flow Rate in the True Aortic Lumen

For each time point, the intensity average in the 2D pcMRI phase image of all pixels within the pROI was multiplied by the tAB area to yield the aortic volumetric flow rate. The aortic blood flow waveform was displayed in a color scheme with high systolic flow in red, accelerating flow in blue/purple, decelerating flow in green and diastolic flow in dark green/brown.

### D. Aortic Boundary Motion Analysis

#### 1. Aortic Center Point Motion

The center of the tAB (ALC) was defined as center of mass of the N lumen boundary points  $(x_i, y_i)$ :

$$ALC = \frac{1}{N} \sum_{i=1}^N \begin{pmatrix} x_i \\ y_i \end{pmatrix}$$

The temporal displacement  $ALC(t)$  was calculated relative to position of the ALC at the time of minimal flow. The

temporal average  $\langle ALC(t) \rangle$  was taken as a measure for the bulk motion of the tAB at this location. Correlation of  $ALC(t)$  with the aortic blood flow waveform was determined with the Pearson correlation coefficient  $r_{ALC}$  (statistical significance for  $p < 0.05$ ).

#### 2. Maximum Positive and Negative Boundary Motion

To exclude the bulk motion of the tAB in the following analysis, a 2D polar coordinate system was defined for each time point with  $ALC(t)$  as origin. Each of the boundary points was then characterized by a radial coordinate (distance  $r$ ) and an angular coordinate (azimuth angle  $\alpha$ ). tAB at minimum aortic flow was identified as the base boundary (figure 1h). At each point  $p$  of the base boundary, the tangent vector  $t_p$  was approximated as:

$$t_p = \sum_{i=1}^2 \begin{pmatrix} \frac{x_{p-i} - x_{p+i}}{i} \\ \frac{y_{p-i} - y_{p+i}}{i} \end{pmatrix}$$

The normal vector  $n_p$  at each point was derived from the tangent vector as

$$n_p = \begin{pmatrix} -t_{y,p} \\ t_{x,p} \end{pmatrix}$$

The corresponding displacement point  $q$  in the direction of the normal vector  $n_p$  for a point  $p$  was identified (figure 1i) by minimizing the cost function  $c(q)$

$$c(q) = (y_p - y_q) + (x_q - x_p) \cdot \frac{n_{p,y}}{n_{p,x}} \cdot \Delta(q)^3$$

with

$$\Delta(q) = \sqrt{(x_p - x_q)^2 + (y_p - y_q)^2}$$

From this displacement, the maximum positive  $d_{max}$  (maximum distension), maximum negative  $d_{min}$  (maximum contraction), and average displacement  $d_{avg}$  of each boundary point was obtained. For a visualization of the boundary motion,  $d_{max}$ ,  $d_{min}$  and  $d_{avg}$  were displayed for all  $p$  in the whole azimuth range (-180 degree - 180 degree) using the same color scheme as the aortic flow waveform.

#### 3. Temporal Average Displacement

Correlation of the tAB displacement averaged over all boundary points ( $AD(t)$ ) with the aortic flow waveform in the true aortic lumen was determined with the Pearson correlation coefficient  $r_{AD(t)}$  (statistical significance for  $< 0.05$ ).

## III. RESULTS

### A. Volumetric Inflow Rates

Flow in the thoracic aorta was dominated by antegrade flow, maximum of 86 ml/sec occurred at 123 msec (figure 2e). In the abdominal aorta, shape of the flow waveform was triphasic, with a maximum of 164 ml/sec at 125 msec and a minimum of -5 ml/sec at 330 msec (figure 3e).

## B. Aortic Wall Motion

### 1. Aortic Lumen Center Point Motion

Average ALC displacement was 0.56 mm (maximum 1.37 mm) in the thoracic aorta and 0.55 mm (maximum 1.37 mm) in the abdominal aorta. ALC motion correlated with aortic flow in the abdominal aorta ( $r_{ALC}=0.88$ , p-value  $4e-6$ ) with forces exerted by the blood flow capable of imposing a bulk motion. No such effect or correlation was observed in the thoracic aorta ( $r_{ALC}=0.28$ , p-value 0.29).

### 2. Maximum Distension and Maximum Contraction

#### a. Thoracic Aorta

Overall maximum distension  $d_{max}$  and maximum contraction  $d_{min}$  were 1.27 mm and -1.64 mm, respectively, for the IS (figure 2a and b) and 1.21 mm and the tAB excluding the IS (figure 2h and i). Maximum distension was observed during maximum flow in the true lumen, i.e. when the dynamic pressure was maximal. Shortly afterwards, maximum contraction of the IS occurred with the flow in the true aortic lumen decelerating. The tAB excluding the IS reached maximum distension at times of maximum flow and maximum contractions at times of decelerating flow, i.e. was pulsating as a whole (with the exception of a small segment (figure 2h and i)).

#### b. Abdominal Aorta

Overall maximum distension  $d_{max}$  and maximum contraction  $d_{min}$  were 0.32 mm and -3.38 mm, respectively, for the IS (figure 3a and b) and 0.52 mm and -1.88 mm for the remaining wall segment (figure 3h and i). The segment

of the IS adjacent to the thrombus appeared mobile and not attached to the thrombus at any location. Maximum distension occurred for the tAB excluding the IS at low flow, maximum contraction during various times during flow acceleration, maximum or decelerating flow (figure 3h and i).

### 3. Average Displacement

The average displacement  $d_{ave}$  of the IS in the thoracic aorta was  $0.09 \pm 0.07$  mm (figure 2c),  $d_{ave}$  for the tAB excluding the IS was  $0.13 \pm 0.07$  (figure 2j). In the abdominal aorta, IS moved on average by  $0.42 \pm 0.23$  mm (figure 3c) and the wall segment excluding the IS by  $0.37 \pm 0.11$  mm (figure 3j).

### 4. Total Average Displacement

The temporal displacement averaged over all boundary points of the IS  $AD(t)$  did not correlate with the shape of the aortic flow waveform in the thoracic aorta  $r_{AD(t)}=0.11$ , p-value = 0.67, figure 2d), but did so negatively in the abdominal aorta ( $r_{AD(t)}=-0.98$ , p-value =  $5e-6$ , figure 3d). A similar behavior was found for the tAB excluding the IS in the thoracic ( $r_{AD(t)}=0.20$ , p-value = 0.44, figure 2k) and abdominal aorta ( $r_{AD(t)}=-0.84$ , p-value =  $6e-6$ , figure 3k). Equation).

## IV. DISCUSSION

The motion of the tAB and the IS in a TB-AD dissection was visualized and quantified with a new image processing algorithm, applied to two sets of clinical 2D pcMRI cross sectional images.

If the wall motion of the true aorta was determined by the dynamic pressure alone, wall displacement should correlate with the true aortic flow waveform. This kind of motion would result in maximum distention of the wall at maximum flow relative to minimum flow. Such a behavior was observed in the thoracic aorta. With thrombus present in the false lumen of the abdominal aorta, wall motion did not correlate with flow in the true lumen, but exhibited an irregular pattern potentially being the result of a complicated interaction between flow and pressures in the true and false lumen. Blood velocities in the false lumen was much lower than in the true lumen (as estimated from the grayscale intensity in the 2D pcMRI images), consequently dynamic pressure was low in the false lumen. Not directly accessible by MRI but suggested by computational fluid dynamics simulations reported previously [12], static pressure may have built-up due to a narrowing of the false lumen caused by thrombus proximal to the re-entrance tear. This pressure raise may have caused the observed irregular motion of the IS and of the aortic wall.

From cine 2-D pcMRI images, Minami et al. quantified diameter changes of the true and false lumen of aortic dissections potentially indicative of IS movement [13]. In a series of ten consecutive cases of acute aortic dissection (six Stanford type A and four Stanford type B) the movement of the intimal flap was characterized by a flap movement index

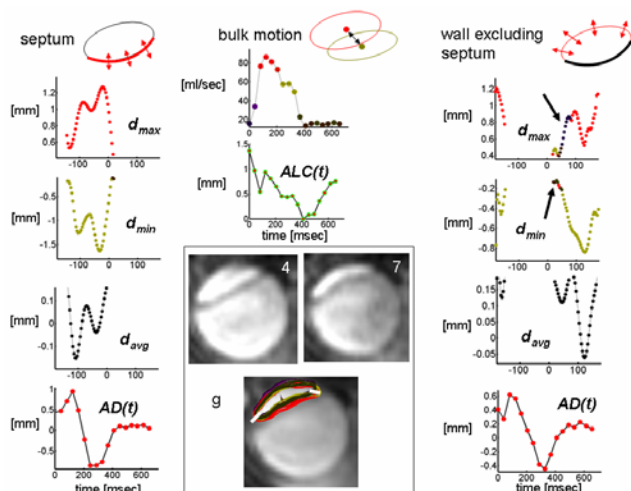


Fig. 2. Results for thoracic aorta. *Left:* Maximum distension  $d_{max}$ , maximum contraction  $d_{min}$ , average displacement  $d_{avg}$  and average wall motion  $AD(t)$  for IS. *Center top:* Aortic flow waveform and bulk motion  $ALC(t)$  of tAB. *Center bottom:* 2D pcMRI magnitude images for time points 4 (maximum inflow) and 7 (decelerating flow) on top and averaged 2D pcMRI magnitude images with tAB overlay below.

*Right:* Maximum distension  $d_{max}$ , maximum contraction  $d_{min}$ , average displacement  $d_{avg}$  and average wall motion  $AD(t)$  for tAB excluding IS. A color scheme was used to mark different times and flow based on the aortic flow waveform. This color scheme was then consistently in the graphs for  $d_{max}$ ,  $d_{min}$  and  $d_{avg}$  and in the overlay of the tAB (center bottom). Units of the x-axis of  $d_{max}$ ,  $d_{min}$  and  $d_{avg}$  is degrees according to the coordinate system illustrated in figure 1h (center row).

(FMI). Maximum and minimum aortic diameters (AD<sub>max</sub>, AD<sub>min</sub>), as well as maximum and minimum false lumen diameters (FD<sub>max</sub>, FD<sub>min</sub>) were measured. FMI was defined as

$(FD_{max}/AD_{max}) - (FD_{min}/AD_{min}) / (FD_{min}/AD_{min}) \times 100(\%)$ . The so defined FMI ranged between 4% and 87% (mean 26.3 +/- 8.6%). The authors concluded that IS movement as characterized by the FMI is a potentially useful parameter in cases with acute aortic dissection to determine whether or not emergency surgery is indicated. [13]. In contrast to the FMI, the IS displacement derived with the here presented algorithm is measured in reference to the center of mass of the true aortic wall. This is a more direct measurement of IS mobility as changes in the diameter of the true and false lumen may depend on other factors.

In an in-vivo study, Wedding et al. demonstrated the feasibility of cine phase contrast MRI for measuring the velocity of the aortic wall and calculated changes in circumferential strain over the cardiac cycle [14]. Ultrasonometry as the gold standard in in-vitro experiments on a deformable vessel phantom was used to confirm the results [14,15]. This method was further validated in the porcine thoracic aorta in-vivo model where the motion of implanted markers in the aortic wall was tracked to validate the results obtained with MRI [16]. These studies demonstrate the reliability of 2D cine 2D pcMRI for quantifying aortic wall motion in-vivo. The results obtained with the here presented algorithms could potentially be used to calculate the radial velocity component of the aortic wall and the IS, additional 2D pcMRI images however have to be acquired to derive tangential velocity components.

Recent technical improvements of pcMRI for time-resolved 3D recording of blood flow velocities in the aorta and other arteries may be used to better understand the fluid dynamics in aortic dissections [17-19].

Limitations of the 2D pcMRI technique consist in its spatial resolution in the mm range, its relatively coarse temporal resolution in the order of tens of milliseconds which is achieved as an average over several heart beats. Partial volume averaging effects are present at the blood-artery wall interface introducing an uncertainty (dependent on the in-plane resolution) about the exact location of the wall. Low and turbulent flow may result in inaccurate measurements of the blood velocity [20].

Despite these limitations, the variety of dynamic parameters accessible with 2D and 3D pcMRI methods, demonstrated and validated, make this imaging technique the method of choice for studying the dynamics of aortic dissections. Further studies are needed to optimize the application of these methods for clinical applications.

#### REFERENCES

[1] J. Y. Bergan, JST, "Aneurysms, Diagnosis and Treatment," New York: Grune & Stratton, 1982.

[2] S. Onitsuka, H. Akashi, K. Tayama, T. Okazaki, K. Ishihara, S. Hiromatsu, and S. Aoyagi, "Long-term outcome and prognostic predictors of medically treated acute type B aortic dissections," *Ann Thorac Surg*, vol. 78, pp. 1268-73, Oct 2004.

[3] H. Ince and C. A. Nienaber, "Diagnosis and management of patients with aortic dissection," *Heart*, vol. 93, pp. 266-70, Feb 2007.

[4] K. A. Eagle and R. W. DeSanctis, "Aortic dissection," *Curr Probl Cardiol*, vol. 14, pp. 225-78, May 1989.

[5] D. Kamalakannan, H. S. Rosman, and K. A. Eagle, "Acute aortic dissection," *Crit Care Clin*, vol. 23, pp. 779-800, vi, Oct 2007.

[6] A. D. Smith and P. Schoenhagen, "CT imaging for acute aortic syndrome," *Cleve Clin J Med*, vol. 75, pp. 7-9, 12, 15-7 passim, Jan 2008.

[7] J. Lin, B. Chen, and J. H. Wang, "Diagnosis of systemic arterial diseases with whole-body 3D contrast-enhanced magnetic resonance angiography," *Chin Med J (Engl)*, vol. 119, pp. 1772-8, Nov 5 2006.

[8] D. F. Guthaner and D. C. Miller, "Digital subtraction angiography of aortic dissection," *AJR Am J Roentgenol*, vol. 141, pp. 157-61, Jul 1983.

[9] P. D. Myerowitz, D. K. Swanson, and W. D. Turnipseed, "Applications of digital subtraction angiography in cardiovascular diagnosis," *Surg Clin North Am*, vol. 65, pp. 423-37, Jun 1985.

[10] S. D. Xu, F. J. Huang, J. H. Du, Y. Li, Z. M. Fan, J. F. Yang, X. Y. Yu, and Z. G. Zhang, "A study of aortic dimension in type B aortic dissection," *Interact Cardiovasc Thorac Surg*, vol. 7, pp. 244-8, Apr 2008.

[11] R. Scott, F. Atkins, and P. V. Harper, "Median Window Filter as a Smoothing-Edge Preserving Technique," *Journal of Nuclear Medicine*, vol. 19, pp. 749-749, 1978.

[12] C. Karmonik, J. X. Bismuth, M. G. Davies, and A. B. Lumsden, "Computational hemodynamics in the human aorta: A computational fluid dynamics study of three cases with patient-specific geometries and inflow rates," *Technol Health Care*, vol. 16, pp. 343-54, 2008.

[13] H. Minami, T. Sugimoto, and M. Okada, "Evaluation of acute aortic dissection by cine-MRI," *Kobe J Med Sci*, vol. 45, pp. 1-11, Feb 1999.

[14] K. L. Wedding, M. T. Draney, R. J. Herfkens, C. K. Zarins, C. A. Taylor, and N. J. Pelc, "Measurement of vessel wall strain using cine phase contrast MRI," *J Magn Reson Imaging*, vol. 15, pp. 418-28, Apr 2002.

[15] M. T. Draney, R. J. Herfkens, T. J. Hughes, N. J. Pelc, K. L. Wedding, C. K. Zarins, and C. A. Taylor, "Quantification of vessel wall cyclic strain using cine phase contrast magnetic resonance imaging," *Ann Biomed Eng*, vol. 30, pp. 1033-45, Sep 2002.

[16] M. T. Draney, F. R. Arko, M. T. Alley, M. Markl, R. J. Herfkens, N. J. Pelc, C. K. Zarins, and C. A. Taylor, "Quantification of vessel wall motion and cyclic strain using cine phase contrast MRI: in vivo validation in the porcine aorta," *Magn Reson Med*, vol. 52, pp. 286-95, Aug 2004.

[17] A. Frydrychowicz, M. Markl, A. Harloff, A. F. Stalder, J. Bock, T. A. Bley, A. Berger, M. F. Russe, C. Schlenzak, J. Hennig, and M. Langer, "[Flow-sensitive in-vivo 4D MR imaging at 3T for the analysis of aortic hemodynamics and derived vessel wall parameters]," *Rofo*, vol. 179, pp. 463-72, May 2007.

[18] T. A. Hope, M. Markl, L. Wigstrom, M. T. Alley, D. C. Miller, and R. J. Herfkens, "Comparison of flow patterns in ascending aortic aneurysms and volunteers using four-dimensional magnetic resonance velocity mapping," *J Magn Reson Imaging*, vol. 26, pp. 1471-9, Dec 2007.

[19] S. Yamashita, H. Isoda, M. Hirano, H. Takeda, S. Inagawa, Y. Takehara, M. T. Alley, M. Markl, N. J. Pelc, and H. Sakahara, "Visualization of hemodynamics in intracranial arteries using time-resolved three-dimensional phase-contrast MRI," *J Magn Reson Imaging*, vol. 25, pp. 473-8, Mar 2007.

[20] K. K. Bernstein MA, Zhou XJ, *Handbook of MRI Pulse Sequences*: Elsevier, Academic Press, 2004.